Figure S1

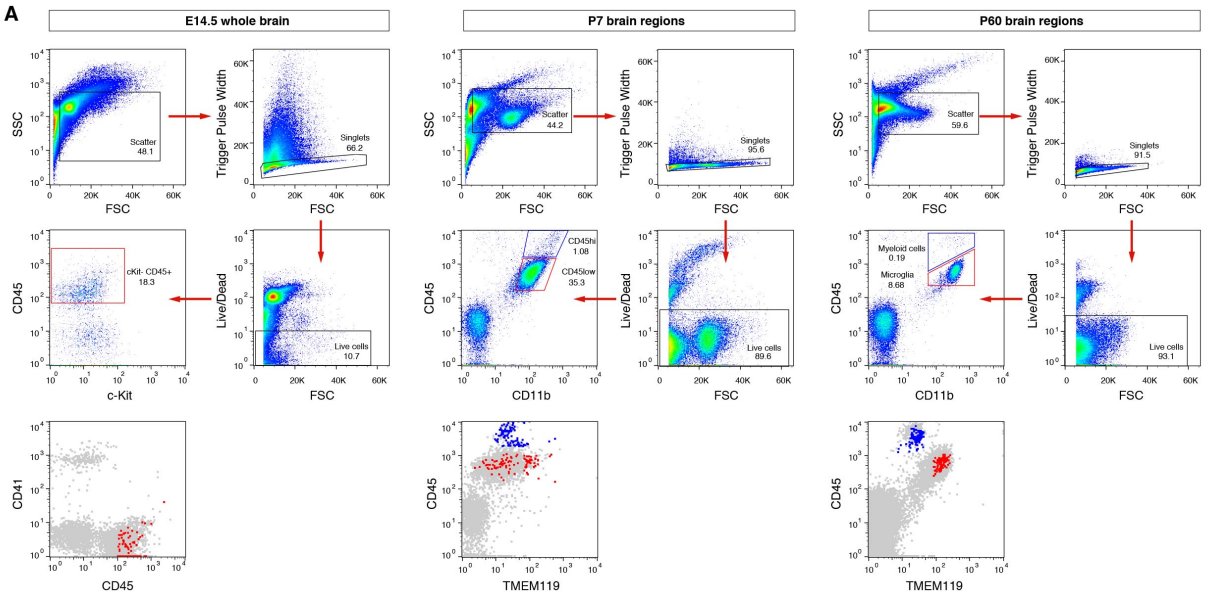

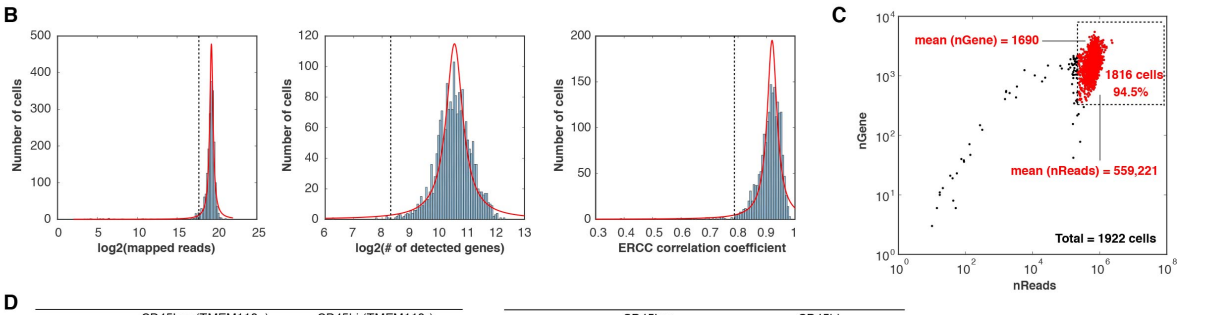

D

P60 cells	CD45low (TMEM119+)		CD45hi (TMEM119-)	
	Sequenced	Passed QC	Sequenced	Passed QC
CTX	77	72	43	38
CB	95	91	53	52
HIP	82	80	29	28
STR	71	70	31	29
OB	59	57	40	38
CP	NA	NA	150	141
Subtotal	384	370	346	326

P7 cells	CD45low		CD45hi	
	Sequenced	Passed QC	Sequenced	Passed QC
CTX	80	48	107	105
CB	78	76	77	75
HIP	85	82	129	125
STR	108	107	63	59
OB	102	96	83	78
CP	NA	NA	136	127
Subtotal	453	409	595	569

E14.5 cells	c-Kit-CD45+	
	Sequenced	Passed QC
Whole brain	144	142

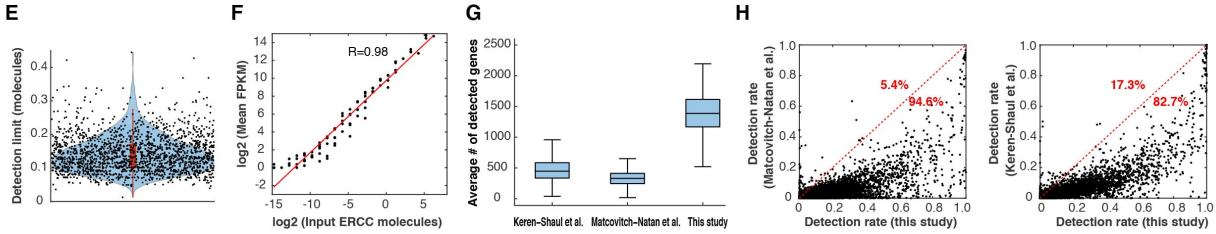

Figure S1. Cell sorting of brain myeloid cells for scRNA-seq and quality assessment, Related to Figure 1.

(A) Representative FACS plots showing gating strategy and the cells sequenced (red or blue dots in the bottom panels) in our study. Microglia and myeloid cells were sorted separately for P7 and P60 stages. (B) Quality control (QC) criteria for the single-cell sequencing data. Fitted curves for histograms of mapped reads, numbers of detected genes and ERCC correlation coefficient (estimating accuracy) are labeled in red. Dashed lines are statistical cutoffs. Cells that passed all three criteria were retained for analysis. (C) Scatter plot highlighting cells that passed QC (red) among all cells sequenced. Each dot is a cell. (D) Summary for the numbers of cells sequenced and cells passed QC (red) from different brain regions and developmental stages. (E) Detection limit of the current scRNA-seq platform showing its single-molecule detection sensitivity for ERCC spike-ins. Each dot represents a cell (See also STAR Methods). (F) Detection accuracy of the current scRNA-seq platform showing its precision based on the high correlation between ERCC input counts and actual sequencing reads. Each dot represents an ERCC molecule. (G) Comparison of the sequencing data for adult microglia with two other studies showing about 3-fold increase in the number of genes detected in each cell by our study. (H) Comparison of the sequencing data for adult microglia with two other studies showing higher detection rates in the sequenced microglia populations for over 80% of genes by our study. Each dot represents a gene.

Figure S2

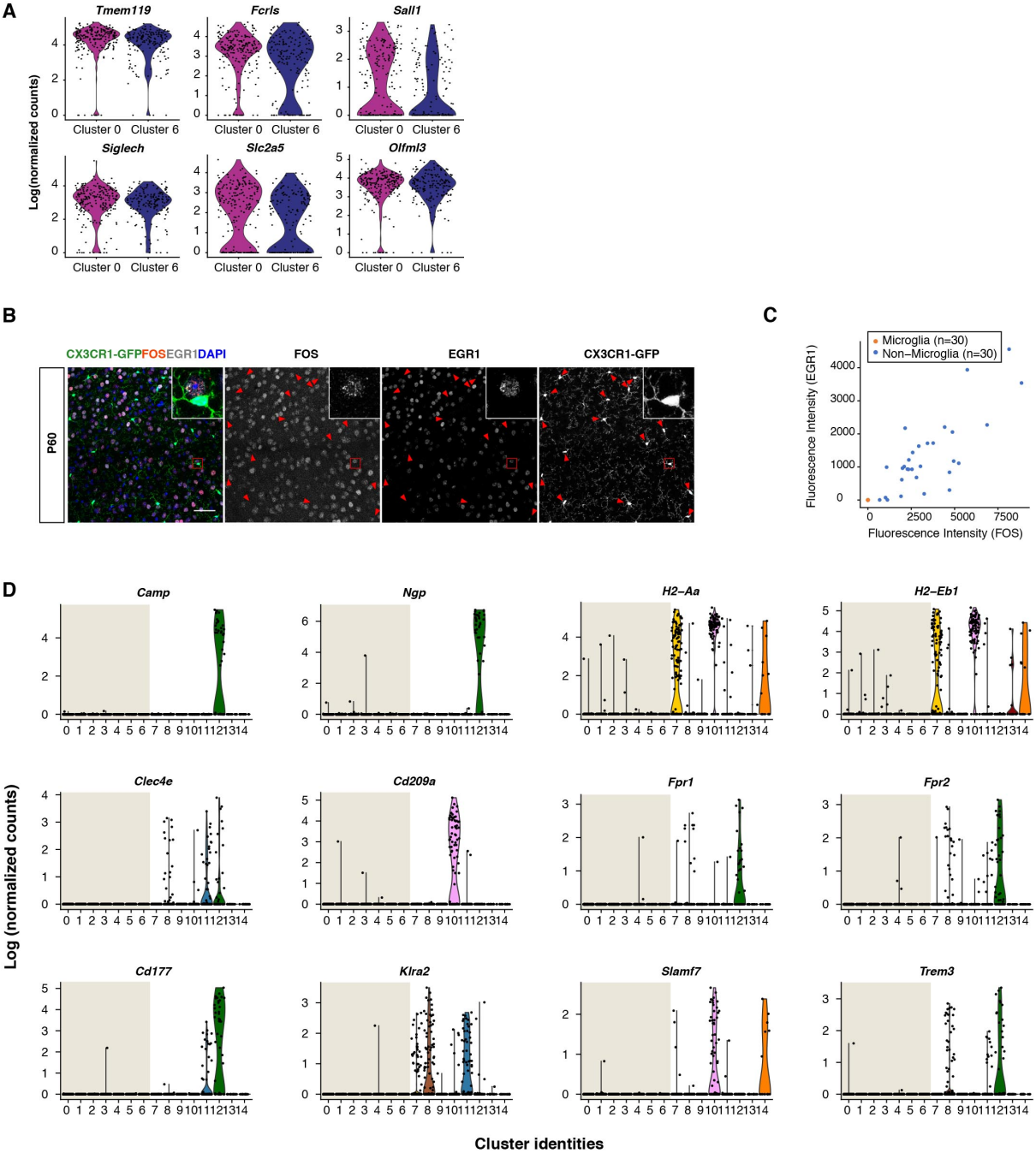
A
Tmem119
Fcrls
Sall1
Siglech
Slc2a5
Olfml3
Log(normalized counts)
Cluster 0
Cluster 6
B
CX3CR1-GFPFOSEGR1DAPI
FOS
EGR1
CX3CR1-GFP
P60
C
Microglia (n=30)
Non−Microglia (n=30)
Fluorescence Intensity (EGR1)
Fluorescence Intensity (FOS)
D
Camp
Ngp
H2−Aa
H2−Eb1
Clec4e
Cd209a
Fpr1
Fpr2
Cd177
Klra2
Slamf7
Trem3
Log (normalized counts)
Cluster identities

Figure S2. Limited transcriptomic heterogeneity of adult homeostatic microglia across brain regions, Related to Figure 3.

(A) Violin plots showing similar expression levels of homeostatic microglial signature genes in two P60 microglia clusters. None of the genes shown were statistically different in expression between the two populations. (B) Immunohistochemistry on fixed sections from adult brains showing negative expression of FOS and EGR1 in microglia (CX3CR1-GFP^{+}, arrow heads), and positive signals from surrounding non-microglia cells. (C) Quantification of fluorescence signals in (B). n=30 cells each, for microglia and non-microglia cells. (D) Violin plots showing that genes reported as being differentially expressed between region-specific microglia in the adult (Grabert et al., 2016) are mainly enriched in non-microglia myeloid cells in our scRNA-seq data. Clusters 0-6 are microglia clusters (shaded in gray). Scale bar in (B) is 50um.

Figure S3

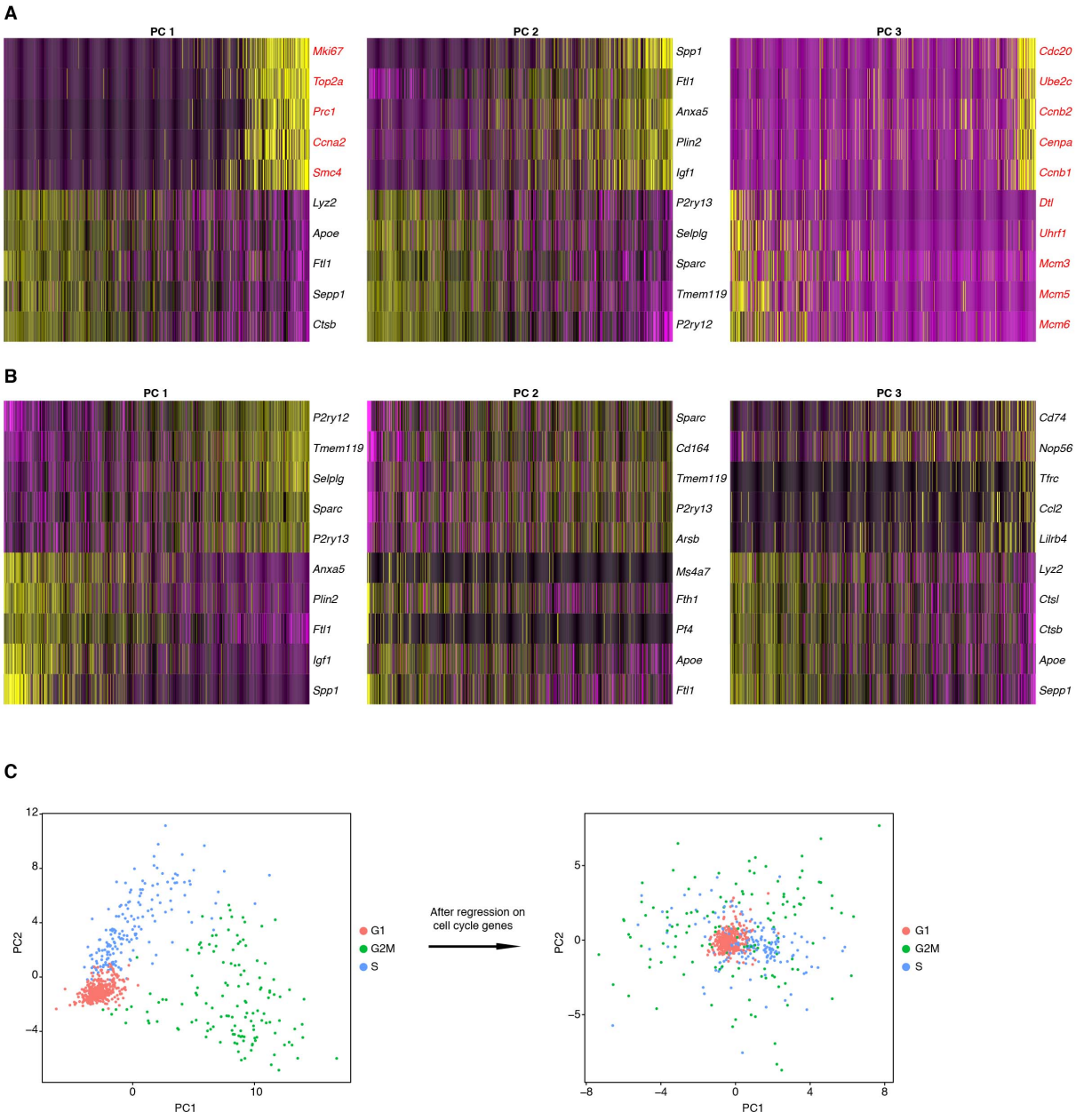
A
PC 1
Mki67
Top2a
Prc1
Ccna2
Smc4
Lyz2
Apoe
Ftl1
Sepp1
Ctsb
PC 2
Spp1
Ftl1
Anxa5
Plin2
Igf1
P2ry13
Selplg
Sparc
Tmem119
P2ry12
PC 3
Cdc20
Ube2c
Ccnb2
Cenpa
Ccnb1
Dtl
Uhrf1
Mcm3
Mcm5
Mcm6
B
PC 1
P2ry12
Tmem119
Selplg
Sparc
P2ry13
Anxa5
Plin2
Ftl1
Igf1
Spp1
PC 2
Sparc
Cd164
Tmem119
P2ry13
Arsb
Ms4a7
Fth1
Pf4
Apoe
Ftl1
PC 3
Cd74
Nop56
Tfrc
Ccl2
Lilrb4
Lyz2
Ctsl
Ctsb
Apoe
Sepp1
C
PC2
PC1
G1
G2M
S
After regression on
cell cycle genes
PC2
PC1
G1
G2M
S

Figure S3. Effect of cell cycle regression on scRNA-seq data for P7 microglia, Related to Figure 4.

(A) Heatmaps showing the top genes from the first three principal components underlying cell-to-cell variations in P7 microglia. Prior to cell cycle regression, known cell cycle related genes (red) were abundant. (B) Heatmaps showing cell cycle regression effect where no known cell cycle related genes were at the top of the first three principal components. (C) Originally, principal component analysis on cell cycle genes separated P7 microglia into different clusters which mostly matched their cell cycle phases (left). After cell cycle regression, cells were no longer separated by cell cycle phases (right).

Figure S4

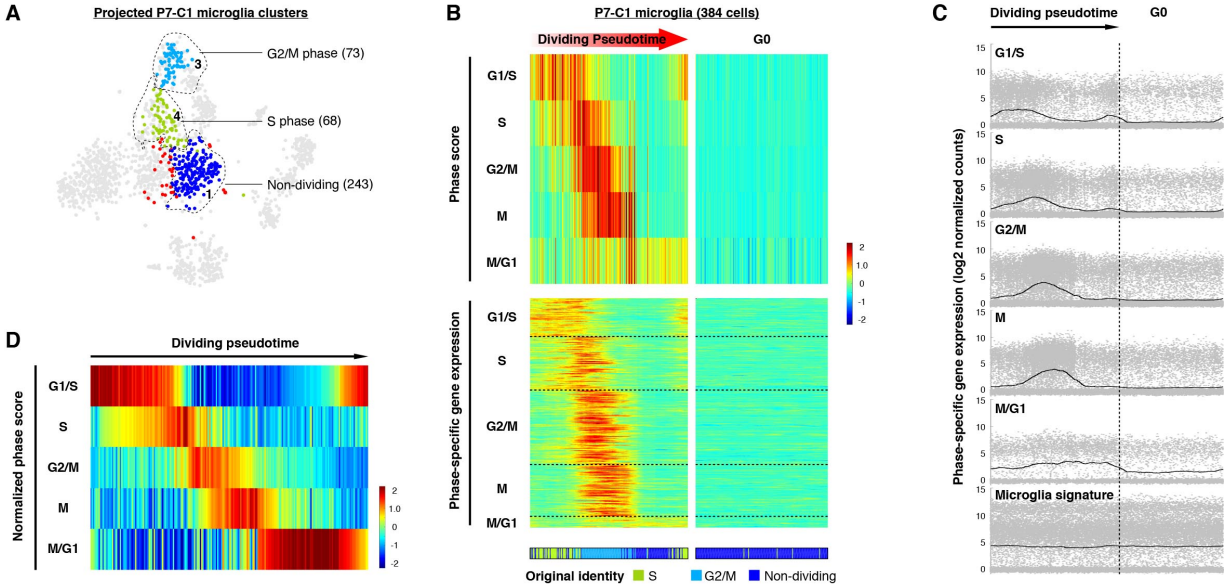

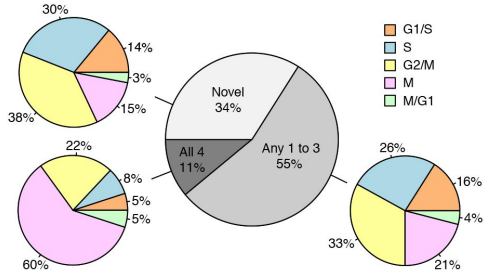

F

Novel cell cycle genes in postnatal PAM (P7-C1)

	Apitd1, *Dnajc9*, ***Dnmt1***, ***Eri1***, *Golt1b*, ***Lig1***, ***Mybl2***, ***Nap1l1***, ***Nup188***, ***Nup43***, ***Pold1***, *Ptma*, ***Rbbp7***, ***Rpa1***, *Slfn9*, *St3gal5*, ***Syce2***
S	*4930427A07Rik*, *4930579G24Rik*, ***Apitd1***, *BC030867*, ***Cenpw***, ***Cep57l1***, ***Chtf18***, *Dck*, *Dek*, *Dnajc9*, ***Dnmt1***, *Dock10*, ***Dynlt1a***, ***Eme1***, ***Eri1***, ***Gen1***, *Gpr165*, ***Gsg2***, ***Hist1h1b***, ***Mybl2***, ***Nap1l1***, *Nrm*, ***Nsl1***, *Paics*, ***Pmf1***, *Ptma*, ***Rad50***, ***Rfwd3***, ***Rpa1***, *Slfn9*, ***Smc1a***, *St3gal5*, *Stmn1*, ***Tk1***
G2/M	*2700099C18Rik*, *4930427A07Rik*, *4930579G24Rik*, *9430015G10Rik*, *Ankle1*, *BC030867*, *Ccdc18*, ***Cenpw***, ***Cep57l1***, *Dek*, *Dock10*, ***Dynlt1a***, ***Eme1***, ***Gen1***, *Gpr165*, ***Gsg2***, ***H2afz***, ***H3f3b***, ***Hist1h1b***, ***Hist1h1d***, ***Hist1h2ab***, ***Hist1h2ae***, ***Hist1h2ai***, ***Hist1h2bg***, ***Hist1h3e***, ***Hist2h3c2***, ***Hmgb1***, *Hmgn2*, *Ilf3*, *Ly6e*, ***Nsl1***, ***Rfwd3***, ***Sass6***, *Selplg*, *Serinc3*, ***Smc1a***, ***Smc2***, ***Snrpb***, ***Spc24***, ***Ssna1***, *Stmn1*, ***Tk1***, ***Ubb***, *Xkr5*
M	*2700094K13Rik*, *2700099C18Rik*, *Ankle1*, *Gm6682*, ***H2afz***, ***H3f3b***, ***Hist1h2bg***, *Hmgn2*, *Ilf3*, ***Miip***, *Mrpl51*, *Ppia*, *Sae1*, *Sh2d3c*, ***Smc2***, ***Ubb***, *Xkr5*
M/G1	*Mtpn*, *Ppia*, ***Rae1***, ***Rbbp7***, *Sae1*, *Taf9*

Figure S4. Phase-specific gene expression of dividing microglia (P7-C1 cluster) along cell cycle pseudotime, Related to Figure 4.

(A) tSNE plots highlight P7-C1 microglia in the original plot (Figure 1C) based on the re-clustering analysis. Cells were color coded the same way as in Figure 1C. Numbers of cells in each cluster were given in parentheses. (B) – (F) are detailed analysis for the 384 P7-C1 microglia shown in (A). (B) Heatmap (upper panel) showing pseudotime ordering of P7-C1 microglia based on raw phase scores. Each column is a cell, and each row denotes raw scores for a specific cell cycle phase along the dividing pseudotime. G0 cells have no dominant phase scores for any phase. Heatmap (lower panel) showing expression levels of individual genes identified as phase-specific by the algorithm. Each column is a cell and each row is a gene. Such ordering is largely consistent with the original cell identities by the clustering analysis as shown in the bottom color-coded bar. (C) Dot plots showing expression levels of phase-specific genes along microglia dividing pseudotime. Genes for each phase were plotted in separate graphs with each dot representing level of expression for a given gene in a given cell. Curves show average expression of all genes assigned to a phase along dividing pseudotime. Expression of microglial signature genes is shown at the bottom. (D) Heatmap showing pseudotime ordering of P7-C1 microglia by using normalized phase scores. (E) The gray pie chart showing overlaps of phase-specific genes identified by the algorithm compared with four published cell cycle gene sets. The novel category shows the percentage of genes found here that were not reported in any of the four datasets. Colored pie charts are breakdowns of the genes from each category based on the phase assignment. (F) Table showing gene names identified as “Novel” in (E). Genes that may play a role in cell division were bolded.

Figure S5

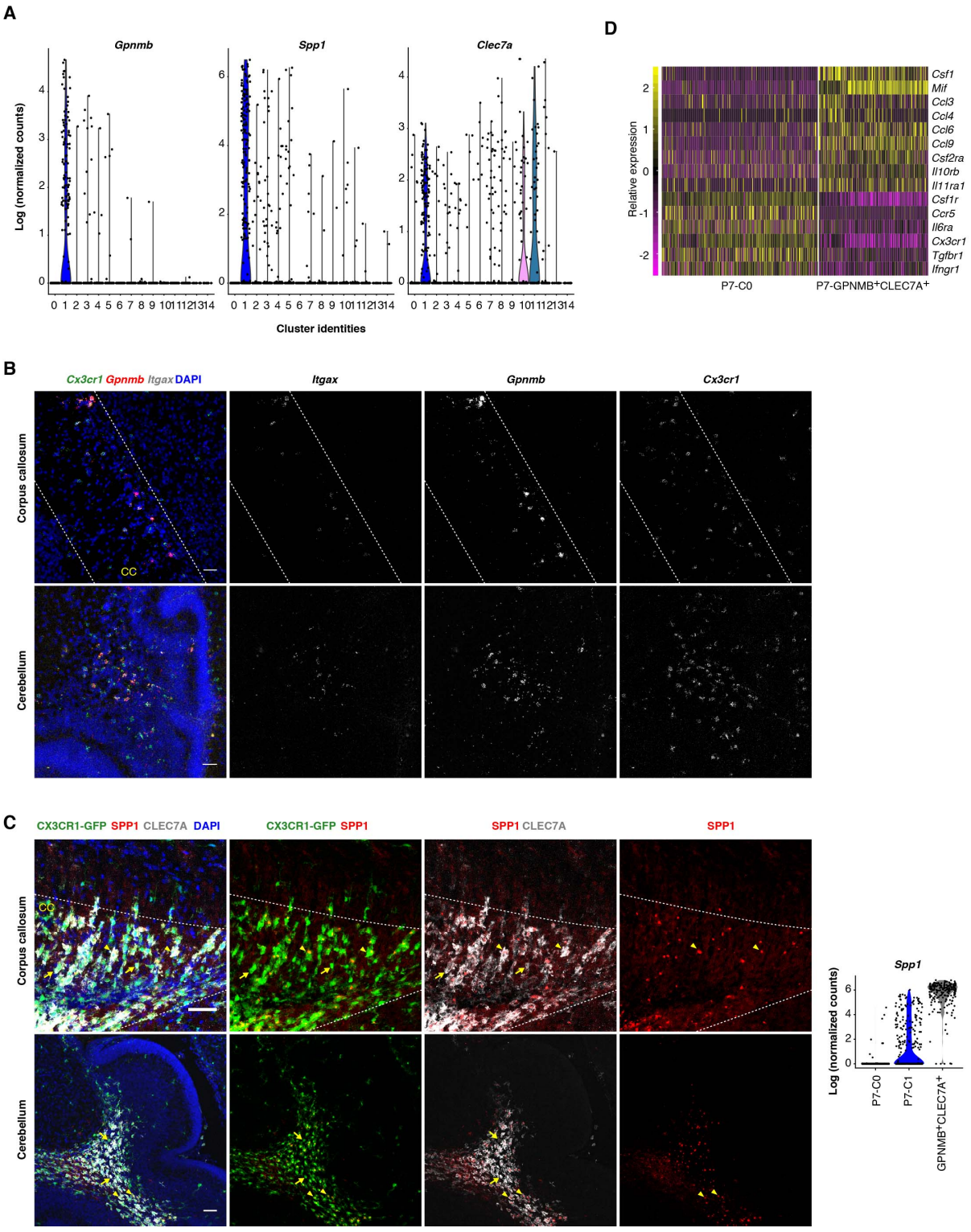
A
Gpnmb
Spp1
Clec7a
Log (normalized counts)
Cluster identities
D
Relative expression
Csf1
Mif
Ccl3
Ccl4
Ccl6
Ccl9
Csf2ra
Il10rb
Il11ra1
Csf1r
Ccr5
Il6ra
Cx3cr1
Tgfbr1
Ifngr1
P7-C0
P7-GPNMB+CLEC7A+
B
Cx3cr1 Gpnmb Itgax DAPI
Itgax
Gpnmb
Cx3cr1
Corpus callosum
Cerebellum
CC
C
CX3CR1-GFP SPP1 CLEC7A DAPI
CX3CR1-GFP SPP1
SPP1 CLEC7A
SPP1
Corpus callosum
Cerebellum
CC
Spp1
Log (normalized counts)
P7-C0
P7-C1
GPNMB+CLEC7A+

Figure S5. Histological validation of early postnatal proliferative region-associated microglia as well as cytokines/chemokines and their receptor expression profiles in these microglia, Related to Figure 6.

(A) Expression of *Gpnmb*, *Spp1* and *Clec7a* in postnatal P7-C1 microglia in comparison with all other sequenced myeloid cells by scRNAseq. See Figure 1C for cluster annotations. (B) RNA *in situ* (RNAscope) validation of *Itgax* expression by P7-C1 microglia (PAM). *Itgax* and *Gpnmb* signals mainly overlapped in the corpus callosum and white matter region of cerebellum, and these cells were also positive for microglia marker *Cx3cr1*. (C) Immunohistochemistry on fixed brain sections showing SPP1 was strongly expressed by a subset of $CLEC7A^{+}$ microglia in the P7 white matter (arrow heads), while $CLEC7A^{+}SPP1^{-}$ microglia were also seen (arrows). Violin plot on the right showing nearly 100% expression of *Spp1* in GPNMB/CLEC7A double positive cells by scRNA-seq. (D) Heatmap showing expression profiles of cytokines/chemokines and their receptors by postnatal microglia. Only genes differentially expressed between postnatal PAM and P7-C0 immature microglia were included. Scale bars in (B) and (C) are 50um.

Figure S6

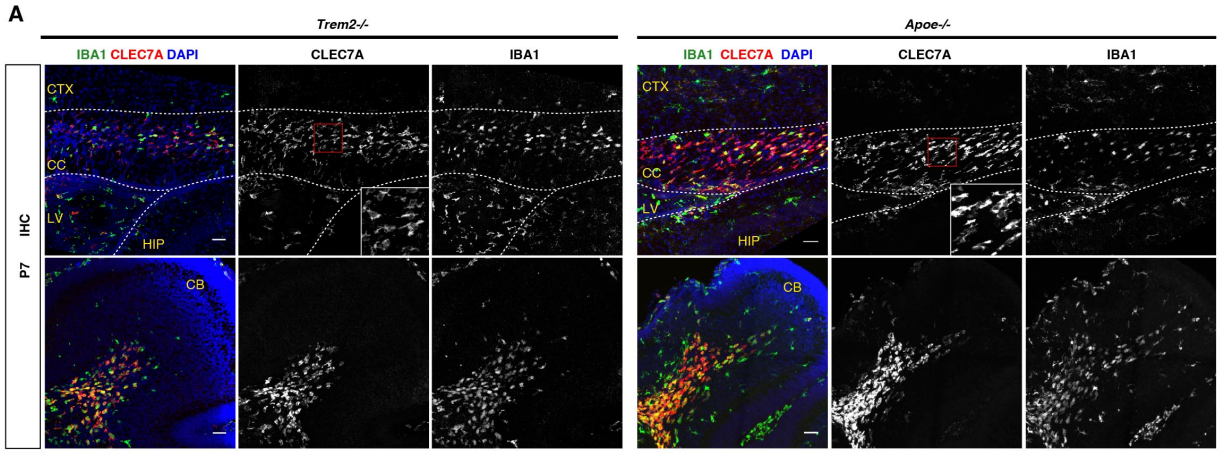

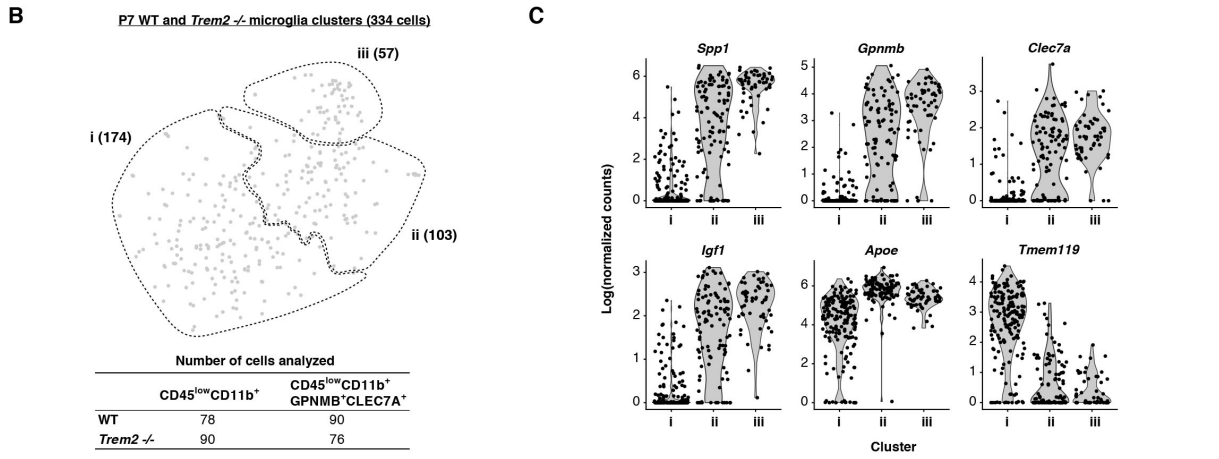

Number of cells analyzed

	$CD45^{low}CD11b^{+}$	$CD45^{low}CD11b^{+}GPNMB^{+}CLEC7A^{+}$
WT	78	90
Trem2 -/-	90	76

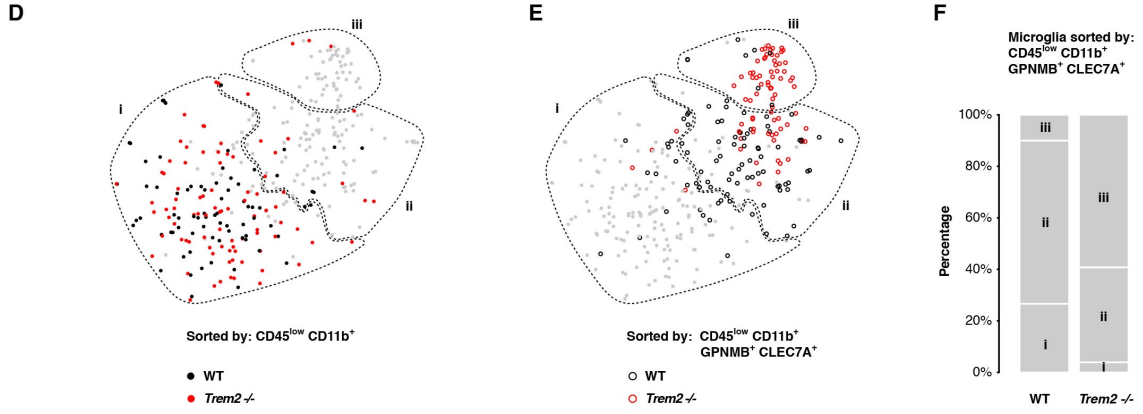

Figure S6. Amoeboid early postnatal PAM, independent of TREM2-APOE regulation, Related to Figure 7.

(A) Immunohistochemistry showing that amoeboid CLEC7A^{+} microglia are present in the corpus callosum and cerebellar white matter region of *Trem2-/-* and *Apoe-/-* mice at P7. CTX: cortex; CC: corpus callosum; LV: lateral ventricle; HIP: hippocampus; CB: cerebellum. Scales bars are 50um. (B) TSNE plot showing 3 clusters of scRNA-seq data of 334 P7 microglia (passed quality control) sorted from C57BL/6J and *Trem2-/-* brains. The table below shows the numbers of cells used for analysis, which were sorted either from the CD45^{low}CD11b^{+} gate or from the CD45^{low}CD11b^{+}GPNMB^{+}CLEC7A^{+} gate (to enrich PAM) in the two genotypes. (C) Violin plots of gene expression showing that cluster (i) represents postnatal immature microglia with low levels of PAM markers (such as *Spp1*, *Gpnmb*, *Clec7a*, *Igf1* and *Apoe*) and high levels of homeostatic markers such as *Tmem119*. Cluster (ii) and cluster (iii) represent PAM to different extent of polarization, with cluster (iii) expressing even higher levels of PAM markers and lower levels of homeostatic markers. (D) Overlaying genotype and sorting gate identities onto the TSNE plot showing that majority of P7 microglia from C57BL/6J and *Trem2-/-* brains are intermingled in the cluster (i). (E) Overlaying genotype and sorting gate identities onto the TSNE plot showing that CD45^{low}CD11b^{+}GPNMB^{+}CLEC7A^{+} microglia sorted from C57BL/6J and *Trem2-/-* brains are mainly found in cluster (ii) and (iii), and *Trem2-/-* cells enriched in this gate seem to preferentially concentrate in cluster (iii), corresponding to higher levels of PAM polarization. (F) Stacked bar plot showing the percentage of CD45^{low}CD11b^{+}GPNMB^{+}CLEC7A^{+} microglia from C57BL/6J or *Trem2-/-* brains in each of the 3 clusters.

Figure S7

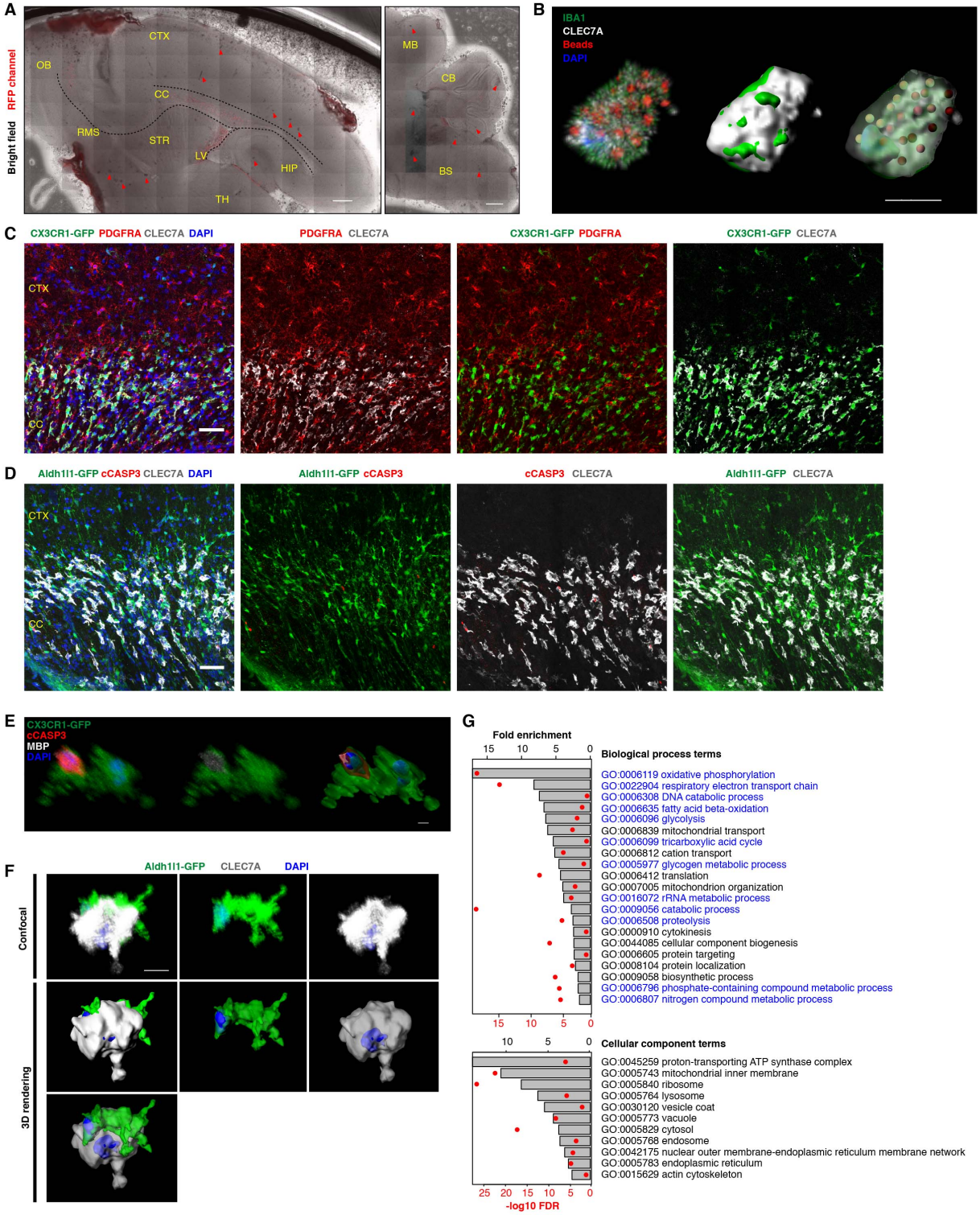
A
RFP channel
Bright field
CTX
OB
CC
RMS
STR
LV
HIP
TH
MB
CB
BS
B
IBA1
CLEC7A
Beads
DAPI
C
CX3CR1-GFP PDGFRA CLEC7A DAPI
PDGFRA CLEC7A
CX3CR1-GFP PDGFRA
CX3CR1-GFP CLEC7A
CTX
CC
D
Aldh1l1-GFP cCASP3 CLEC7A DAPI
Aldh1l1-GFP cCASP3
cCASP3 CLEC7A
Aldh1l1-GFP CLEC7A
CTX
CC
E
CX3CR1-GFP
cCASP3
MBP
DAPI
F
Aldh1l1-GFP CLEC7A DAPI
Confocal
3D rendering
G
Fold enrichment
15 10 5 0
Biological process terms
GO:0006119 oxidative phosphorylation
GO:0022904 respiratory electron transport chain
GO:0006308 DNA catabolic process
GO:0006635 fatty acid beta-oxidation
GO:0006096 glycolysis
GO:0006839 mitochondrial transport
GO:0006099 tricarboxylic acid cycle
GO:0006812 cation transport
GO:0005977 glycogen metabolic process
GO:0006412 translation
GO:0007005 mitochondrion organization
GO:0016072 rRNA metabolic process
GO:0009056 catabolic process
GO:0006508 proteolysis
GO:0000910 cytokinesis
GO:0044085 cellular component biogenesis
GO:0006605 protein targeting
GO:0008104 protein localization
GO:0009058 biosynthetic process
GO:0006796 phosphate-containing compound metabolic process
GO:0006807 nitrogen compound metabolic process
15 10 5 0
10 5 0
Cellular component terms
GO:0045259 proton-transporting ATP synthase complex
GO:0005743 mitochondrial inner membrane
GO:0005840 ribosome
GO:0005764 lysosome
GO:0030120 vesicle coat
GO:0005773 vacuole
GO:0005829 cytosol
GO:0005768 endosome
GO:0042175 nuclear outer membrane-endoplasmic reticulum membrane network
GO:0005783 endoplasmic reticulum
GO:0015629 actin cytoskeleton
25 20 15 10 5 0
-log10 FDR

Figure S7. Phagocytosis of newly formed oligodendrocytes and possibly astrocytes by early postnatal PAM, Related to Figure 8.

(A) Slice culturing sections after 4hr beads incubation and prior to washing demonstrating broad distribution of beads across brain regions in the phagocytosis assay. Dark spots (arrow heads) were congregated beads in areas where little phagocytosis was observed in microglia. Fluorescent beads were already visible in the developing white matter regions at this lower magnification of light microscopy. (B) 3D construction of a beads-eating CLEC7A$^+$ microglia. Spherical beads (red) were readily seen inside of the cell. (C) Little interaction between early postnatal PAM and PDGFRA$^+$ oligodendrocyte precursor cells in the corpus callosum shown by immunostaining. (D) Physical interaction between early postnatal PAM and Aldh1l1-GFP$^+$ astrocytes in the corpus callosum (right panel). Aldh1l1-GFP$^+$ astrocytes did not overlap with cCASP3$^+$ signals, which were sometimes inside CLEC7A$^+$ microglia (middle two panels). (E) 3D reconstruction (right panel) of an early postnatal PAM phagocytosing a dying (cCASP3$^+$) MBP$^+$ oligodendrocyte. Also see Movie S2. (F) 3D reconstruction of an early postnatal PAM interacting with an Aldh1l1-GFP$^+$ astrocyte. Over 30% of astrocyte volume overlapped with the CLEC7A signal calculated by Imaris. (G) GO term analysis showing enriched terms for “Biological Process” and “Cellular Component” in P7-GPNMB$^+$CLEC7A$^+$ microglia (PAM) by PANTHER software. Fold enrichment was shown by bars, and -log10 FDR (false discovery rate) was shown by red dots. Terms related to metabolism were highlighted in blue. CTX: cortex; CC: corpus callosum; STR: striatum; HIP: hippocampus; LV: lateral ventricle; OB: olfactory bulb; TH: thalamus; RMS: rostral migratory stream; MB: midbrain; CB: cerebellum; BS: brain stem. Scale bars: 500um in (A); 10um in (B), (E) and (F); 50um in (C) and (D).